Fermilab-Pub-10-403-E

Precise study of the Z/γ^* boson transverse momentum distribution in $p\bar{p}$ collisions using a novel technique

V.M. Abazov,[35] B. Abbott,[73] M. Abolins,[62] B.S. Acharya,[29] M. Adams,[48] T. Adams,[46] G.D. Alexeev,[35] G. Alkhazov,[39] A. Alton[a],[61] G. Alverson,[60] G.A. Alves,[2] L.S. Ancu,[34] M. Aoki,[47] Y. Arnoud,[14] M. Arov,[57] A. Askew,[46] B. Åsman,[40] O. Atramentov,[65] C. Avila,[8] J. BackusMayes,[80] F. Badaud,[13] L. Bagby,[47] B. Baldin,[47] D.V. Bandurin,[46] S. Banerjee,[29] E. Barberis,[60] P. Baringer,[55] J. Barreto,[2] J.F. Bartlett,[47] U. Bassler,[18] V. Bazterra,[48] S. Beale,[6] A. Bean,[55] M. Begalli,[3] M. Begel,[71] C. Belanger-Champagne,[40] L. Bellantoni,[47] S.B. Beri,[27] G. Bernardi,[17] R. Bernhard,[22] I. Bertram,[41] M. Besançon,[18] R. Beuselinck,[42] V.A. Bezzubov,[38] P.C. Bhat,[47] V. Bhatnagar,[27] G. Blazey,[49] S. Blessing,[46] K. Bloom,[64] A. Boehnlein,[47] D. Boline,[70] T.A. Bolton,[56] E.E. Boos,[37] G. Borissov,[41] T. Bose,[59] A. Brandt,[76] O. Brandt,[23] R. Brock,[62] G. Brooijmans,[68] A. Bross,[47] D. Brown,[17] J. Brown,[17] X.B. Bu,[7] D. Buchholz,[50] M. Buehler,[79] V. Buescher,[24] V. Bunichev,[37] S. Burdin[b],[41] T.H. Burnett,[80] C.P. Buszello,[42] B. Calpas,[15] E. Camacho-Pérez,[32] M.A. Carrasco-Lizarraga,[32] B.C.K. Casey,[47] H. Castilla-Valdez,[32] S. Chakrabarti,[70] D. Chakraborty,[49] K.M. Chan,[53] A. Chandra,[78] G. Chen,[55] S. Chevalier-Théry,[18] D.K. Cho,[75] S.W. Cho,[31] S. Choi,[31] B. Choudhary,[28] T. Christoudias,[42] S. Cihangir,[47] D. Claes,[64] J. Clutter,[55] M. Cooke,[47] W.E. Cooper,[47] M. Corcoran,[78] F. Couderc,[18] M.-C. Cousinou,[15] A. Croc,[18] D. Cutts,[75] M. Ćwiok,[30] A. Das,[44] G. Davies,[42] K. De,[76] S.J. de Jong,[34] E. De La Cruz-Burelo,[32] F. Déliot,[18] M. Demarteau,[47] R. Demina,[69] D. Denisov,[47] S.P. Denisov,[38] S. Desai,[47] K. DeVaughan,[64] H.T. Diehl,[47] M. Diesburg,[47] A. Dominguez,[64] T. Dorland,[80] A. Dubey,[28] L.V. Dudko,[37] D. Duggan,[65] A. Duperrin,[15] S. Dutt,[27] A. Dyshkant,[49] M. Eads,[64] D. Edmunds,[62] J. Ellison,[45] V.D. Elvira,[47] Y. Enari,[17] S. Eno,[58] H. Evans,[51] A. Evdokimov,[71] V.N. Evdokimov,[38] G. Facini,[60] T. Ferbel,[58,69] F. Fiedler,[24] F. Filthaut,[34] W. Fisher,[62] H.E. Fisk,[47] M. Fortner,[49] H. Fox,[41] S. Fuess,[47] T. Gadfort,[71] A. Garcia-Bellido,[69] V. Gavrilov,[36] P. Gay,[13] W. Geist,[19] W. Geng,[15,62] D. Gerbaudo,[66] C.E. Gerber,[48] Y. Gershtein,[65] G. Ginther,[47,69] G. Golovanov,[35] A. Goussiou,[80] P.D. Grannis,[70] S. Greder,[19] H. Greenlee,[47] Z.D. Greenwood,[57] E.M. Gregores,[4] G. Grenier,[20] Ph. Gris,[13] J.-F. Grivaz,[16] A. Grohsjean,[18] S. Grünendahl,[47] M.W. Grünewald,[30] F. Guo,[70] J. Guo,[70] G. Gutierrez,[47] P. Gutierrez,[73] A. Haas[c],[68] S. Hagopian,[46] J. Haley,[60] L. Han,[7] K. Harder,[43] A. Harel,[69] J.M. Hauptman,[54] J. Hays,[42] T. Head,[43] T. Hebbeker,[21] D. Hedin,[49] H. Hegab,[74] A.P. Heinson,[45] U. Heintz,[75] C. Hensel,[23] I. Heredia-De La Cruz,[32] K. Herner,[61] G. Hesketh,[60] M.D. Hildreth,[53] R. Hirosky,[79] T. Hoang,[46] J.D. Hobbs,[70] B. Hoeneisen,[12] M. Hohlfeld,[24] S. Hossain,[73] Z. Hubacek,[10] N. Huske,[17] V. Hynek,[10] I. Iashvili,[67] R. Illingworth,[47] A.S. Ito,[47] S. Jabeen,[75] M. Jaffré,[16] S. Jain,[67] D. Jamin,[15] R. Jesik,[42] K. Johns,[44] M. Johnson,[47] D. Johnston,[64] A. Jonckheere,[47] P. Jonsson,[42] J. Joshi,[27] A. Juste[d],[47] K. Kaadze,[56] E. Kajfasz,[15] D. Karmanov,[37] P.A. Kasper,[47] I. Katsanos,[64] R. Kehoe,[77] S. Kermiche,[15] N. Khalatyan,[47] A. Khanov,[74] A. Kharchilava,[67] Y.N. Kharzheev,[35] D. Khatidze,[75] M.H. Kirby,[50] J.M. Kohli,[27] A.V. Kozelov,[38] J. Kraus,[62] A. Kumar,[67] A. Kupco,[11] T. Kurča,[20] V.A. Kuzmin,[37] J. Kvita,[9] S. Lammers,[51] G. Landsberg,[75] P. Lebrun,[20] H.S. Lee,[31] S.W. Lee,[54] W.M. Lee,[47] J. Lellouch,[17] L. Li,[45] Q.Z. Li,[47] S.M. Lietti,[5] J.K. Lim,[31] D. Lincoln,[47] J. Linnemann,[62] V.V. Lipaev,[38] R. Lipton,[47] Y. Liu,[7] Z. Liu,[6] A. Lobodenko,[39] M. Lokajicek,[11] P. Love,[41] H.J. Lubatti,[80] R. Luna-Garcia[e],[32] A.L. Lyon,[47] A.K.A. Maciel,[2] D. Mackin,[78] R. Madar,[18] R. Magaña-Villalba,[32] S. Malik,[64] V.L. Malyshev,[35] Y. Maravin,[56] J. Martínez-Ortega,[32] R. McCarthy,[70] C.L. McGivern,[55] M.M. Meijer,[34] A. Melnitchouk,[63] D. Menezes,[49] P.G. Mercadante,[4] M. Merkin,[37] A. Meyer,[21] J. Meyer,[23] N.K. Mondal,[29] G.S. Muanza,[15] M. Mulhearn,[79] E. Nagy,[15] M. Naimuddin,[28] M. Narain,[75] R. Nayyar,[28] H.A. Neal,[61] J.P. Negret,[8] P. Neustroev,[39] S.F. Novaes,[5] T. Nunnemann,[25] G. Obrant,[39] J. Orduna,[32] N. Osman,[42] J. Osta,[53] G.J. Otero y Garzón,[1] M. Owen,[43] M. Padilla,[45] M. Pangilinan,[75] N. Parashar,[52] V. Parihar,[75] S.K. Park,[31] J. Parsons,[68] R. Partridge[c],[75] N. Parua,[51] A. Patwa,[71] B. Penning,[47] M. Perfilov,[37] K. Peters,[43] Y. Peters,[43] G. Petrillo,[69] P. Pétroff,[16] R. Piegaia,[1] J. Piper,[62] M.-A. Pleier,[71] P.L.M. Podesta-Lerma[f],[32] V.M. Podstavkov,[47] M.-E. Pol,[2] P. Polozov,[36] A.V. Popov,[38] M. Prewitt,[78] D. Price,[51] S. Protopopescu,[71] J. Qian,[61] A. Quadt,[23] B. Quinn,[63] M.S. Rangel,[2] K. Ranjan,[28] P.N. Ratoff,[41] I. Razumov,[38] P. Renkel,[77] P. Rich,[43] M. Rijssenbeek,[70] I. Ripp-Baudot,[19] F. Rizatdinova,[74] M. Rominsky,[47] C. Royon,[18] P. Rubinov,[47] R. Ruchti,[53] G. Safronov,[36] G. Sajot,[14] A. Sánchez-Hernández,[32] M.P. Sanders,[25] B. Sanghi,[47] A.S. Santos,[5] G. Savage,[47] L. Sawyer,[57] T. Scanlon,[42] R.D. Schamberger,[70] Y. Scheglov,[39] H. Schellman,[50] T. Schliephake,[26]

S. Schlobohm,[80] C. Schwanenberger,[43] R. Schwienhorst,[62] J. Sekaric,[55] H. Severini,[73] E. Shabalina,[23] V. Shary,[18] A.A. Shchukin,[38] R.K. Shivpuri,[28] V. Simak,[10] V. Sirotenko,[47] P. Skubic,[73] P. Slattery,[69] D. Smirnov,[53] K.J. Smith,[67] G.R. Snow,[64] J. Snow,[72] S. Snyder,[71] S. Söldner-Rembold,[43] L. Sonnenschein,[21] A. Sopczak,[41] M. Sosebee,[76] K. Soustruznik,[9] B. Spurlock,[76] J. Stark,[14] V. Stolin,[36] D.A. Stoyanova,[38] E. Strauss,[70] M. Strauss,[73] D. Strom,[48] L. Stutte,[47] P. Svoisky,[73] M. Takahashi,[43] A. Tanasijczuk,[1] W. Taylor,[6] M. Titov,[18] V.V. Tokmenin,[35] D. Tsybychev,[70] B. Tuchming,[18] C. Tully,[66] P.M. Tuts,[68] L. Uvarov,[39] S. Uvarov,[39] S. Uzunyan,[49] R. Van Kooten,[51] W.M. van Leeuwen,[33] N. Varelas,[48] E.W. Varnes,[44] I.A. Vasilyev,[38] P. Verdier,[20] L.S. Vertogradov,[35] M. Verzocchi,[47] M. Vesterinen,[43] D. Vilanova,[18] P. Vint,[42] P. Vokac,[10] H.D. Wahl,[46] M.H.L.S. Wang,[69] J. Warchol,[53] G. Watts,[80] M. Wayne,[53] M. Weber[g],[47] L. Welty-Rieger,[50] M. Wetstein,[58] A. White,[76] D. Wicke,[24] M.R.J. Williams,[41] G.W. Wilson,[55] S.J. Wimpenny,[45] M. Wobisch,[57] D.R. Wood,[60] T.R. Wyatt,[43] Y. Xie,[47] C. Xu,[61] S. Yacoob,[50] R. Yamada,[47] W.-C. Yang,[43] T. Yasuda,[47] Y.A. Yatsunenko,[35] Z. Ye,[47] H. Yin,[7] K. Yip,[71] H.D. Yoo,[75] S.W. Youn,[47] J. Yu,[76] S. Zelitch,[79] T. Zhao,[80] B. Zhou,[61] J. Zhu,[61] M. Zielinski,[69] D. Zieminska,[51] and L. Zivkovic[68]

(The D0 Collaboration*)

[1] *Universidad de Buenos Aires, Buenos Aires, Argentina*
[2] *LAFEX, Centro Brasileiro de Pesquisas Físicas, Rio de Janeiro, Brazil*
[3] *Universidade do Estado do Rio de Janeiro, Rio de Janeiro, Brazil*
[4] *Universidade Federal do ABC, Santo André, Brazil*
[5] *Instituto de Física Teórica, Universidade Estadual Paulista, São Paulo, Brazil*
[6] *Simon Fraser University, Vancouver, British Columbia, and York University, Toronto, Ontario, Canada*
[7] *University of Science and Technology of China, Hefei, People's Republic of China*
[8] *Universidad de los Andes, Bogotá, Colombia*
[9] *Charles University, Faculty of Mathematics and Physics, Center for Particle Physics, Prague, Czech Republic*
[10] *Czech Technical University in Prague, Prague, Czech Republic*
[11] *Center for Particle Physics, Institute of Physics, Academy of Sciences of the Czech Republic, Prague, Czech Republic*
[12] *Universidad San Francisco de Quito, Quito, Ecuador*
[13] *LPC, Université Blaise Pascal, CNRS/IN2P3, Clermont, France*
[14] *LPSC, Université Joseph Fourier Grenoble 1, CNRS/IN2P3, Institut National Polytechnique de Grenoble, Grenoble, France*
[15] *CPPM, Aix-Marseille Université, CNRS/IN2P3, Marseille, France*
[16] *LAL, Université Paris-Sud, CNRS/IN2P3, Orsay, France*
[17] *LPNHE, Universités Paris VI and VII, CNRS/IN2P3, Paris, France*
[18] *CEA, Irfu, SPP, Saclay, France*
[19] *IPHC, Université de Strasbourg, CNRS/IN2P3, Strasbourg, France*
[20] *IPNL, Université Lyon 1, CNRS/IN2P3, Villeurbanne, France and Université de Lyon, Lyon, France*
[21] *III. Physikalisches Institut A, RWTH Aachen University, Aachen, Germany*
[22] *Physikalisches Institut, Universität Freiburg, Freiburg, Germany*
[23] *II. Physikalisches Institut, Georg-August-Universität Göttingen, Göttingen, Germany*
[24] *Institut für Physik, Universität Mainz, Mainz, Germany*
[25] *Ludwig-Maximilians-Universität München, München, Germany*
[26] *Fachbereich Physik, Bergische Universität Wuppertal, Wuppertal, Germany*
[27] *Panjab University, Chandigarh, India*
[28] *Delhi University, Delhi, India*
[29] *Tata Institute of Fundamental Research, Mumbai, India*
[30] *University College Dublin, Dublin, Ireland*
[31] *Korea Detector Laboratory, Korea University, Seoul, Korea*
[32] *CINVESTAV, Mexico City, Mexico*
[33] *FOM-Institute NIKHEF and University of Amsterdam/NIKHEF, Amsterdam, The Netherlands*
[34] *Radboud University Nijmegen/NIKHEF, Nijmegen, The Netherlands*
[35] *Joint Institute for Nuclear Research, Dubna, Russia*
[36] *Institute for Theoretical and Experimental Physics, Moscow, Russia*
[37] *Moscow State University, Moscow, Russia*
[38] *Institute for High Energy Physics, Protvino, Russia*
[39] *Petersburg Nuclear Physics Institute, St. Petersburg, Russia*
[40] *Stockholm University, Stockholm and Uppsala University, Uppsala, Sweden*
[41] *Lancaster University, Lancaster LA1 4YB, United Kingdom*
[42] *Imperial College London, London SW7 2AZ, United Kingdom*
[43] *The University of Manchester, Manchester M13 9PL, United Kingdom*
[44] *University of Arizona, Tucson, Arizona 85721, USA*

[45]University of California Riverside, Riverside, California 92521, USA
[46]Florida State University, Tallahassee, Florida 32306, USA
[47]Fermi National Accelerator Laboratory, Batavia, Illinois 60510, USA
[48]University of Illinois at Chicago, Chicago, Illinois 60607, USA
[49]Northern Illinois University, DeKalb, Illinois 60115, USA
[50]Northwestern University, Evanston, Illinois 60208, USA
[51]Indiana University, Bloomington, Indiana 47405, USA
[52]Purdue University Calumet, Hammond, Indiana 46323, USA
[53]University of Notre Dame, Notre Dame, Indiana 46556, USA
[54]Iowa State University, Ames, Iowa 50011, USA
[55]University of Kansas, Lawrence, Kansas 66045, USA
[56]Kansas State University, Manhattan, Kansas 66506, USA
[57]Louisiana Tech University, Ruston, Louisiana 71272, USA
[58]University of Maryland, College Park, Maryland 20742, USA
[59]Boston University, Boston, Massachusetts 02215, USA
[60]Northeastern University, Boston, Massachusetts 02115, USA
[61]University of Michigan, Ann Arbor, Michigan 48109, USA
[62]Michigan State University, East Lansing, Michigan 48824, USA
[63]University of Mississippi, University, Mississippi 38677, USA
[64]University of Nebraska, Lincoln, Nebraska 68588, USA
[65]Rutgers University, Piscataway, New Jersey 08855, USA
[66]Princeton University, Princeton, New Jersey 08544, USA
[67]State University of New York, Buffalo, New York 14260, USA
[68]Columbia University, New York, New York 10027, USA
[69]University of Rochester, Rochester, New York 14627, USA
[70]State University of New York, Stony Brook, New York 11794, USA
[71]Brookhaven National Laboratory, Upton, New York 11973, USA
[72]Langston University, Langston, Oklahoma 73050, USA
[73]University of Oklahoma, Norman, Oklahoma 73019, USA
[74]Oklahoma State University, Stillwater, Oklahoma 74078, USA
[75]Brown University, Providence, Rhode Island 02912, USA
[76]University of Texas, Arlington, Texas 76019, USA
[77]Southern Methodist University, Dallas, Texas 75275, USA
[78]Rice University, Houston, Texas 77005, USA
[79]University of Virginia, Charlottesville, Virginia 22901, USA
[80]University of Washington, Seattle, Washington 98195, USA

(Dated: October 1, 2010)

Using 7.3 fb^{-1} of $p\bar{p}$ collisions collected by the D0 detector at the Fermilab Tevatron, we measure the distribution of the variable ϕ_η^*, which probes the same physical effects as the Z/γ^* boson transverse momentum, but is less susceptible to the effects of experimental resolution and efficiency. A QCD prediction is found to describe the general features of the ϕ_η^* distribution, but is unable to describe its detailed shape or dependence on boson rapidity. A prediction that includes a broadening of transverse momentum for small values of the parton momentum fraction is strongly disfavored.

PACS numbers: 12.38.Qk, 13.85.Qk, 14.70.Hp

Z/γ^* bosons are produced at hadron colliders via quark-antiquark annihilation. Their decays to e^+e^- and $\mu^+\mu^-$ can be detected with little background and the phenomenology is simplified by the absence of color flow between the initial and final states, thus providing an excellent testing ground for QCD predictions. Resummation techniques [1] allow calculations of the distribution of Z/γ^* boson transverse momentum, $p_T^{\ell\ell}$, within the framework of perturbative QCD, even at relatively low $p_T^{\ell\ell}$ (e.g., $p_T^{\ell\ell} < 30$ GeV). However, additional non-perturbative form factors must be determined in global fits to experimental data [2]. An increase of these form factors for $x < 10^{-2}$, where x is the parton momentum fraction, was suggested [3] to improve the description of hadron production observed in deep inelastic electron-proton scattering at HERA. Since vector boson production corresponds typically to parton $x < 10^{-2}$ at the LHC, these modified form factors would lead to a broadening of the expected vector boson transverse momentum distributions [4]. This "small-x broadening" would influ-

*with visitors from [a]Augustana College, Sioux Falls, SD, USA, [b]The University of Liverpool, Liverpool, UK, [c]SLAC, Menlo Park, CA, USA, [d]ICREA/IFAE, Barcelona, Spain, [e]Centro de Investigacion en Computacion - IPN, Mexico City, Mexico, [f]ECFM, Universidad Autonoma de Sinaloa, Culiacán, Mexico, and [g]Universität Bern, Bern, Switzerland.

ence the measurement of the W boson mass as well as searches for Higgs bosons and physics beyond the standard model at the LHC. It is important to study quantitatively such x-dependencies at the Tevatron, where they can be probed using the dependence of the $p_T^{\ell\ell}$ distribution on boson rapidity [5].

In the region of low $p_T^{\ell\ell}$, the precision of the most recent measurements at the Tevatron [6, 7] was dominated by uncertainties in correcting for experimental resolution and efficiency. Furthermore, the choice of bin widths was restricted by experimental resolution rather than event statistics. The variable a_T, which corresponds to the component of $p_T^{\ell\ell}$ that is transverse to the dilepton thrust axis, $\hat{t}$, has been proposed as an alternative analysing variable that allows us to study the issues discussed above, but is less susceptible than the $p_T^{\ell\ell}$ to detector effects [8]. Figure 1 illustrates this and other relevant variables defined below. The a_T distribution was subsequently calculated to next-to-leading-log (NLL) accuracy using resummation techniques [9]. Additional analysing variables with even better experimental resolution have recently been proposed and studied [10]. The optimal variable was found to be ϕ_η^*, which is defined as:

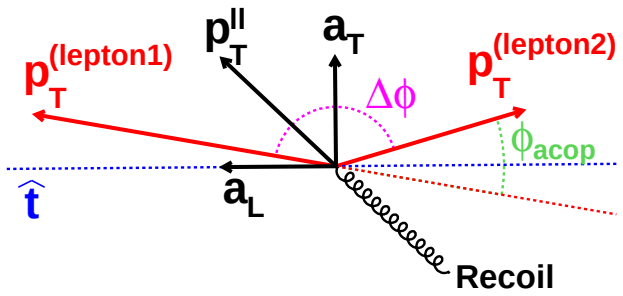

FIG. 1: Illustration of the variables defined in the text and used to analyse the dilepton transverse momentum.

$$\phi_\eta^* = \tan\left(\phi_{\rm acop}/2\right)\sin(\theta_\eta^*),$$

where $\phi_{\rm acop}$ is the acoplanarity angle, given by: $\phi_{\rm acop} = \pi - \Delta\phi^{\ell\ell}$, and $\Delta\phi^{\ell\ell}$ is the difference in azimuthal angle, ϕ, between the two lepton candidates. The variable θ_η^* is a measure of the scattering angle of the leptons with respect to the proton beam direction in the rest frame of the dilepton system. It is defined [10] by: $\cos(\theta_\eta^*) = \tanh\left[\left(\eta^- - \eta^+\right)/2\right]$, where η^- and η^+ are the pseudorapidities [5] of the negatively and positively charged lepton, respectively.

The variable ϕ_η^* is highly correlated with the quantity $a_T/m_{\ell\ell}$, where $m_{\ell\ell}$ is the dilepton invariant mass. Since $\phi_{\rm acop}$ and θ_η^* depend exclusively on the directions of the two leptons, which are measured with a precision of a milliradian or better, ϕ_η^* is experimentally very well measured compared to any quantities that rely on the momenta of the leptons.

We present a measurement of the normalized ϕ_η^* distribution, $(1/\sigma) \times (d\sigma/d\phi_\eta^*)$, in bins of $|y|$, using 7.3 fb^{-1} of $p\bar{p}$ collisions collected by the D0 detector at the Fermilab Tevatron. The ϕ_η^* distributions are measured in both dielectron and dimuon events and are corrected for experimental resolution and efficiency. We correct back to the level of observable, generator-level particles; that is, we apply kinematic selection criteria at the particle level that match those applied in the selection of candidate events in the data [11]. Particle level electrons are defined as the four-vector sum of any electrons and photons within a cone of $\Delta\mathcal{R} = \sqrt{(\Delta\eta)^2 + (\Delta\phi)^2} < 0.2$ around an electron, where $\Delta\eta$ ($\Delta\phi$) is the distance in η (ϕ) from the particle level electron; this mimics the measurement of electron energy in the calorimeter. Particle level muons are defined after QED final state radiation; this mimics the measurement of muon momentum in the tracking detector. The kinematic selection criteria are: electrons must satisfy $p_T > 20$ GeV and $|\eta| < 1.1$ or $1.5 < |\eta| < 3$; muons must satisfy $p_T > 15$ GeV and $|\eta| < 2$; $m_{\ell\ell}$ must fall within the range 70–110 GeV.

The corrected data are compared to predictions from the Monte Carlo (MC) program ResBos [12] with the above kinematic selection criteria applied at the particle level. ResBos generates Z/γ^* boson events with initial state QCD corrections to next-to-leading order (NLO) and NLL accuracy together with: a non-perturbative form factor, whose width is controlled primarily by the parameter g_2 (with default value $[0.68^{+0.02}_{-0.01}]$ GeV^2)[2]; an additional next-to-NLO (NNLO) K-factor [13]; CTEQ6.6 NLO parton distribution functions (PDFs) [14]; and QED radiative corrections from photos [15]. The QCD factorization and renormalization scales are set event by event to the mass of the Z/γ^* boson propagator.

The D0 detector [16] consists of: silicon microstrip and central fiber tracking detectors, located within a 2 T superconducting solenoid; a liquid-argon/uranium sampling calorimeter; and an outer muon system consisting of tracking and scintillation detectors located before and after 1.8 T toroids. Candidate dielectron events are required to satisfy a trigger based on the identification of a single electron and to contain two clusters reconstructed in the calorimeter with a transverse and longitudinal shower profile consistent with that expected of an electron. The calorimeter is housed in three separate cryostats; this has the effect that electron identification is degraded in the region $1.1 < |\eta| < 1.5$. Candidate dimuon events are required to satisfy a trigger based on the identification of a single muon and to contain two muons reconstructed either in the outer muon system, or as an energy deposit consistent with the passage of a minimum-ionizing particle in the calorimeter. In order to ensure an accurate measurement of the lepton directions at the point of production, the two lepton candidates are required to be matched to a pair of oppositely charged particle tracks reconstructed in the

central tracking detectors. Candidate leptons resulting from misidentified hadrons or produced by the decay of hadrons are suppressed by requiring that they be isolated from other particles in the event and, in the case of electrons with $|\eta| < 1.1$, by requiring the energy measured in the calorimeter and the momentum measured in the central tracking detectors to be consistent. Contamination from cosmic ray muons is strongly suppressed by a requirement that the muons originate from the $p\bar{p}$ collision point and by rejecting events in which the two muon candidates are back to back in η. In total, 455k dielectron events and 511k dimuon events are selected.

The corrections to the observed ϕ^*_η distribution for experimental resolution and efficiency are evaluated using Z/γ^* boson MC events that are generated with PYTHIA [17] and passed through a GEANT-based [18] simulation of the detector. These fully simulated MC events are re-weighted at the generator level in two dimensions ($p_T^{\ell\ell}$ and $|y|$) to match the predictions of RESBOS. In addition, adjustments are made to improve the accuracy of the following aspects of the detector simulation: electron energy and muon p_T scale and resolution; track ϕ and η resolutions; trigger efficiencies; and relevant offline reconstruction and selection efficiencies. Variations in the above adjustments to the underlying physics and the detector simulation are included in the assessment of the systematic uncertainties on the correction factors.

The systematic uncertainties due to electron energy and muon p_T scale and resolution are small, and arise only due to the kinematic requirements in the event selection. The measured ϕ^*_η distribution is, however, susceptible to modulations in ϕ of the lepton identification and trigger efficiencies, which result, e.g., from detector module boundaries in the calorimeter and muon systems. Particular care has been taken (a) in the choice of lepton identification criteria in order to minimize such modulations and (b) to ensure that such modulations are well simulated in the MC. For example, the requirements imposed on shower profile are much looser than those usually employed in electron identification within D0, because tight requirements are particularly inefficient in the regions close to module boundaries in the calorimeter. Similarly, the inclusion of muon candidates identified in the calorimeter reduces the effect of gaps between modules in the outer muon system. Accurate modelling of the angular resolution of the central tracking detectors is another crucial aspect of this analysis. The resolution in ϕ and η is measured in the data using cosmic ray muons that traverse the detector, since these should produce events containing two tracks that are exactly back to back except for the effect of detector resolution.

Backgrounds from $Z \to \tau^-\tau^+$, $W \to \ell\nu$ (+jets), and $WW \to \ell\nu\ell\nu$ are simulated using PYTHIA. Background from top quark pair events is simulated with ALPGEN [19], with PYTHIA used for parton showering. Background from multijet events is estimated from data. The total fraction of background events is 0.26% for the dielectron channel, and 0.38% for the dimuon channel.

Since the experimental resolution in ϕ^*_η is narrower than the chosen bin widths, the fractions of accepted events that fall within the same bin in ϕ^*_η at the particle level and reconstructed detector level in the MC are high, having typical (lowest) values of around 98% (92%). Therefore, simple bin-by-bin corrections of the ϕ^*_η distribution are sufficient. In almost all ϕ^*_η bins the total systematic uncertainty is substantially smaller than the statistical uncertainty.

Figure 2 shows the corrected particle level ϕ^*_η distributions together with predictions from RESBOS. Figure 3 shows the ratio of the corrected ϕ^*_η distributions to the RESBOS predictions in both the dielectron and dimuon channels. The general shape of the distributions is broadly described by RESBOS over the full range in ϕ^*_η. However, the small statistical uncertainties resulting from the large dilepton data sets, combined with the fine binning and small systematic uncertainties resulting from the use of ϕ^*_η as the analysing variable, reveal differences between the data and RESBOS. Since the particle level definitions for electrons and muons to which the data are corrected are slightly different, Fig. 3 represents the most appropriate way to demonstrate the consistency of the dielectron and dimuon data. Given that the experimental acceptance corrections are very different in the two channels, this consistency represents a powerful cross check of the corrected distributions.

The results of fits for the value of g_2, separately in each $|y|$ bin and channel, are shown in Table I. It can be seen that the fitted values of g_2 show a monotonic decrease with increasing $|y|$ for both channels. That is, the width of the ϕ^*_η distribution becomes narrower with increasing $|y|$ faster in the data than is predicted by RESBOS. This is the opposite of the behavior expected from the small-x broadening hypothesis [3, 4]. Figure 3 confirms that the prediction from RESBOS with small-x broadening is in poor agreement with data. It can also be seen that choosing the g_2 value (0.66 GeV^2) that best describes the average behavior of the data over all $|y|$ bins and channels has little effect on the level of agreement with data.

Channel	$\lvert y\rvert < 1$	$1 < \lvert y\rvert < 2$	$\lvert y\rvert > 2$
ee	0.644 ± 0.013	0.619 ± 0.017	0.550 ± 0.048
$\mu\mu$	0.670 ± 0.012	0.645 ± 0.019	–

TABLE I: Value of g_2 (GeV^2) that best describes the corrected data in each $|y|$ bin and channel.

A previous measurement [7] showed that, for central rapidities, RESBOS underestimates the number of Z/γ^* bosons at high $p_T^{\ell\ell}$ by about 10%. This is consistent with the deviations seen at high values of ϕ^*_η in Fig. 3 (a).

In summary, using 7.3 fb^{-1} of $p\bar{p}$ collisions collected

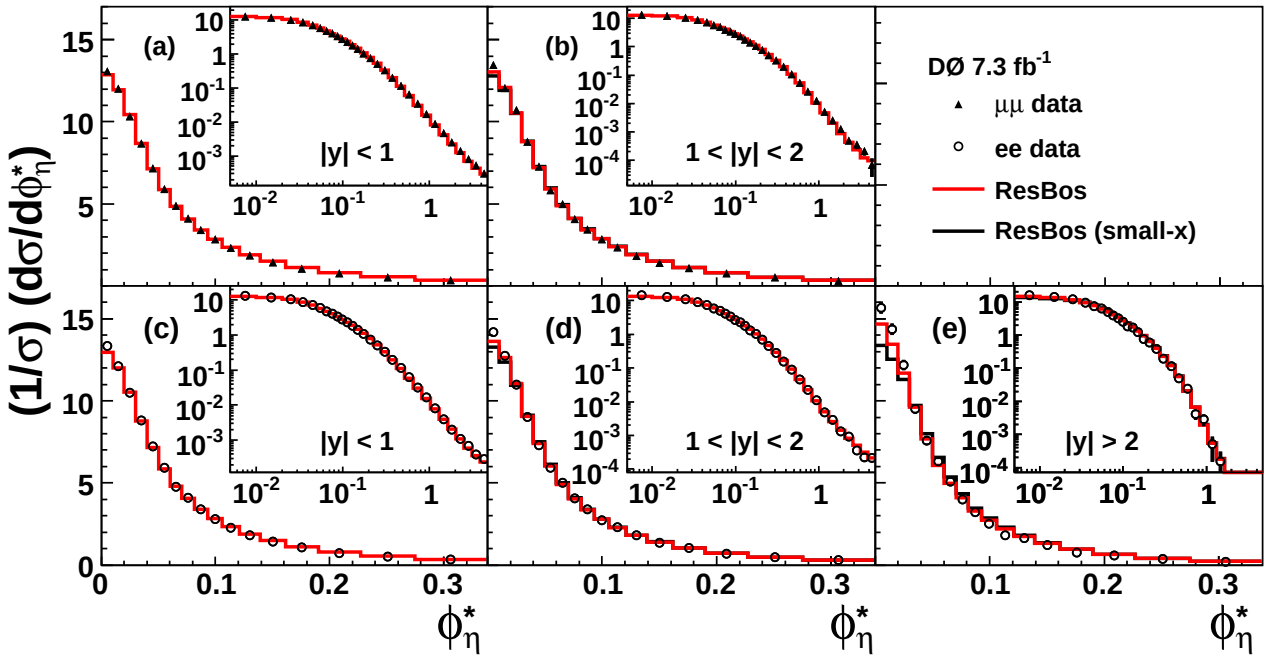

FIG. 2: (color online) Corrected distributions of $(1/\sigma) \times (d\sigma/d\phi^*_\eta)$ for dimuon events with (a) $|y| < 1$ and (b) $1 < |y| < 2$; and dielectron events with (c) $|y| < 1$, (d) $1 < |y| < 2$ and (e) $|y| > 2$. The larger plots show the restricted range $0 < \phi^*_\eta < 0.34$ and the insets show the full range of ϕ^*_η. The predictions from ResBos are shown as the red histogram and from ResBos with small-x broadening as the black histogram [which is visible principally in (e)].

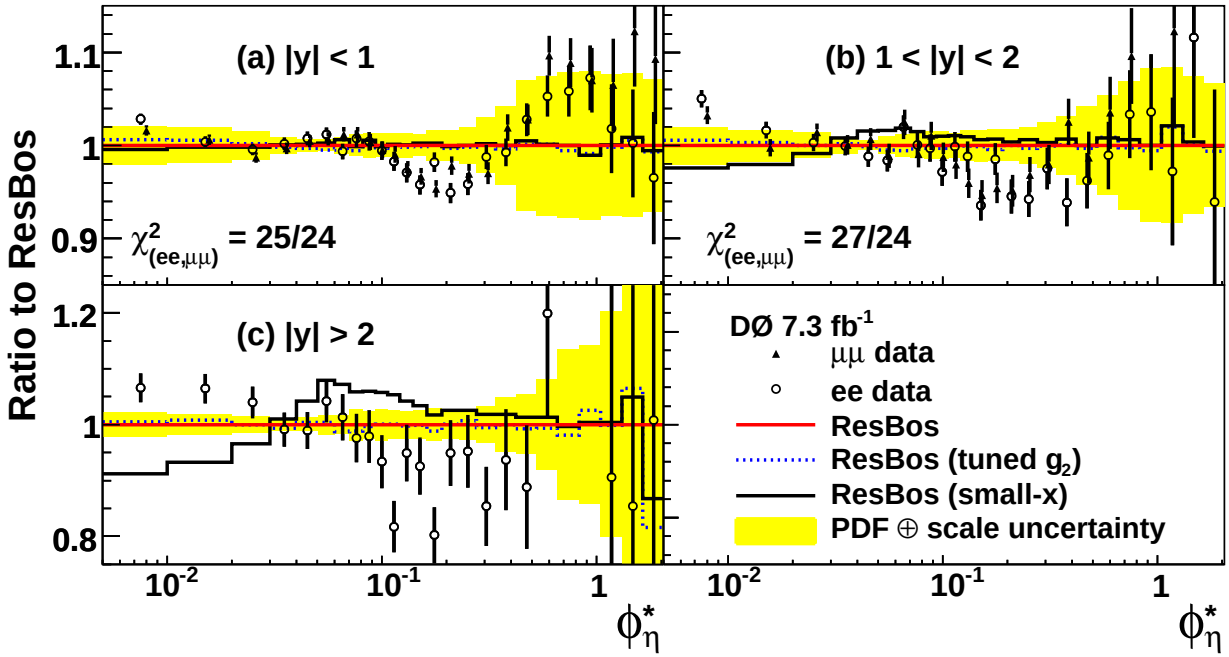

FIG. 3: (color online) Ratio of the corrected distributions of $(1/\sigma) \times (d\sigma/d\phi^*_\eta)$ to ResBos for: (a) $|y| < 1$, (b) $1 < |y| < 2$ and (c) $|y| > 2$. Statistical and systematic uncertainties are combined in quadrature. In (a) and (b) a χ^2 for the comparison of the dielectron and dimuon data, $\chi^2_{(ee/\mu\mu)}$, is calculated assuming uncorrelated uncertainties. The yellow band around the ResBos prediction represents the quadrature sum of uncertainty due to PDFs (evaluated using the CTEQ6.6 NLO error PDFs [14]) and the uncertainty due to the QCD scale (evaluated by varying the factorization and renormalization scales simultaneously by a factor of two). Also shown are the changes to the ResBos predictions when g_2 is set to 0.66 (dotted blue line) and when the small-x broadening option is enabled (solid black line).

by the D0 detector at the Fermilab Tevatron, we have studied with unprecedented precision the $p_T^{\ell\ell}$ distribution of Z/γ^* bosons in dielectron and dimuon final states. In bins of boson rapidity, the normalised cross section is measured as a function of the variable ϕ_η^*. Predictions from RESBOS are unable to describe the detailed shape of the corrected data, and a prediction that includes the effect of small-x broadening is strongly disfavored.

Tables of corrected $(1/\sigma) \times (d\sigma/d\phi_\eta^*)$ distributions for each $|y|$ bin and channel are provided [20].

We thank the staffs at Fermilab and collaborating institutions, and acknowledge support from the DOE and NSF (USA); CEA and CNRS/IN2P3 (France); FASI, Rosatom and RFBR (Russia); CNPq, FAPERJ, FAPESP and FUNDUNESP (Brazil); DAE and DST (India); Colciencias (Colombia); CONACyT (Mexico); KRF and KOSEF (Korea); CONICET and UBACyT (Argentina); FOM (The Netherlands); STFC and the Royal Society (United Kingdom); MSMT and GACR (Czech Republic); CRC Program and NSERC (Canada); BMBF and DFG (Germany); SFI (Ireland); The Swedish Research Council (Sweden); and CAS and CNSF (China).

[1] J. Collins, D. Soper, G. Sterman, Nucl. Phys. B **250**, 199 (1985).
[2] F. Landry, R. Brock, P. M. Nadolsky, C. P. Yuan, Phys. Rev. D **67**, 073016 (2003).
[3] P. Nadolsky, D. R. Stump, C. P. Yuan, Phys. Rev. D **64**, 114011 (2001).
[4] S. Berge, P. Nadolsky, F. Olness, C. P. Yuan, Phys. Rev. D **72**, 033015 (2005). The parameters that control small-x broadening in RESBOS are set to the values given here.
[5] Rapidity is defined by $y = (1/2) \ln \left[(E - p_z) / (E + p_z) \right]$, where E is the energy and p_z is the momentum component parallel to the proton beam axis.. Pseudorapidity is defined by $\eta = -\ln [\tan(\theta/2)]$, where θ is the polar angle.
[6] D0 Collaboration, V. M. Abazov *et al.*, Phys. Rev. Lett. **100**, 102002 (2008).
[7] D0 Collaboration, V. M. Abazov *et al.*, arXiv:1006.0618 [hep-ex], accepted for publication in Phys. Lett. B (2010).
[8] M. Vesterinen, T. R. Wyatt, Nucl. Instrum. Methods Phys. Res. A **602**, 432 (2009).
[9] A. Banfi, M. Dasgupta, R. Delgado, J. High Energy Phys. **12**, 022 (2009).
[10] A. Banfi, S. Redford, M. Vesterinen, P. Waller, T. R. Wyatt, arXiv:1009.1580 [hep-ex], submitted to Eur. Phys. J. C (2010).
[11] Following the recommendations of, J. M. Butterworth *et al.*, arXiv:1003.1643 [hep-ph] (2010).
[12] C. Balazs, C. P. Yuan, Phys. Rev. D **56**, 5558 (1997).
[13] P. B. Arnold, M. H. Reno, Nucl. Phys. B **319**, 37 (1989); B **330**, 284(E) (1990).
[14] P. Nadolsky *et al.*, Phys. Rev. **D** 78, 013004 (2008).
[15] E. Barberio and Z. Was, Comput. Phys. Commun. **79**, 291 (1994).
[16] D0 Collaboration, V. M. Abazov *et al.*, Nucl. Instrum. Methods Phys. Res. A **565**, 463 (2006).
[17] T. Sjöstrand *et al.*, Comp. Phys. Comm. **135**, 238 (2001).
[18] S. Agostinelli *et al.*., Nucl. Instrum. Methods Phys. Res. A **506**, 250 (2003).
[19] M. L. Mangano *et al.*, JHEP **0307**, 001 (2003).
[20] See the supplementary material in the appendix.

Supplementary Material

Tables II–VI show the values of the corrected $(1/\sigma) \times (d\sigma/d\phi^*_\eta)$ distributions for each $|y|$ bin and channel. The first uncertainty is statistical and the second is systematic. The data are corrected back to the particle level, corresponding to the kinematic cuts and definitions of particle level leptons as described in the text. The integral of $(1/\sigma) \times (d\sigma/d\phi^*_\eta)$ for ϕ^*_η in the range 0–4.749 is normalised to unity separately for each $|y|$ bin and channel, with the exception of the dielectron channel for $|y| > 2$ in which the integral is normalised in the ϕ^*_η range 0–2.049 .

TABLE II: The corrected $(1/\sigma) \times (d\sigma/d\phi^*_\eta)$ distribution for the dielectron channel and $|y| < 1$.

bin	range	$(1/\sigma) \times (d\sigma/d\phi^*_\eta)$
1	0.000-0.010	13.242 ± 0.065 ± 0.020
2	0.010-0.020	12.006 ± 0.062 ± 0.012
3	0.020-0.030	10.429 ± 0.058 ± 0.012
4	0.030-0.040	8.756 ± 0.053 ± 0.008
5	0.040-0.050	7.183 ± 0.048 ± 0.007
6	0.050-0.060	5.911 ± 0.043 ± 0.005
7	0.060-0.071	4.762 ± 0.039 ± 0.005
8	0.071-0.081	4.070 ± 0.035 ± 0.003
9	0.081-0.093	3.387 ± 0.031 ± 0.005
10	0.093-0.106	2.806 ± 0.026 ± 0.004
11	0.106-0.121	2.279 ± 0.022 ± 0.003
12	0.121-0.139	1.830 ± 0.018 ± 0.003
13	0.139-0.162	1.414 ± 0.014 ± 0.003
14	0.162-0.190	1.084 ± 0.011 ± 0.002
15	0.190-0.227	0.750 ± 0.008 ± 0.002
16	0.227-0.275	0.513 ± 0.006 ± 0.001
17	0.275-0.337	0.333 ± 0.004 ± 0.001
18	0.337-0.418	0.197 ± 0.003 ± 0.000
19	0.418-0.523	0.115 ± 0.002 ± 0.000
bin	range	$(1/\sigma) \times (d\sigma/d\phi^*_\eta)$ (×1000)
20	0.523-0.657	61.731 ± 1.238 ± 0.090
21	0.657-0.827	32.115 ± 0.798 ± 0.080
22	0.827-1.041	16.496 ± 0.509 ± 0.071
23	1.041-1.309	7.960 ± 0.324 ± 0.171
24	1.309-1.640	3.882 ± 0.203 ± 0.087
25	1.640-2.049	2.006 ± 0.133 ± 0.056
26	2.049-2.547	1.068 ± 0.090 ± 0.033
27	2.547-3.151	0.702 ± 0.067 ± 0.028
28	3.151-3.878	0.389 ± 0.045 ± 0.015
29	3.878-4.749	0.284 ± 0.036 ± 0.013

TABLE III: The corrected $(1/\sigma) \times (d\sigma/d\phi^*_\eta)$ distribution for the dielectron channel and $1 < |y| < 2$.

bin	range	$(1/\sigma) \times (d\sigma/d\phi^*_\eta)$
1	0.000-0.010	14.235 ± 0.104 ± 0.053
2	0.010-0.020	12.782 ± 0.099 ± 0.046
3	0.020-0.030	11.035 ± 0.092 ± 0.030
4	0.030-0.040	9.023 ± 0.083 ± 0.019
5	0.040-0.050	7.268 ± 0.074 ± 0.011
6	0.050-0.060	5.911 ± 0.067 ± 0.007
7	0.060-0.071	4.988 ± 0.061 ± 0.006
8	0.071-0.081	4.029 ± 0.053 ± 0.007
9	0.081-0.093	3.346 ± 0.047 ± 0.006
10	0.093-0.106	2.696 ± 0.040 ± 0.008
11	0.106-0.121	2.267 ± 0.034 ± 0.010
12	0.121-0.139	1.780 ± 0.027 ± 0.010
13	0.139-0.162	1.308 ± 0.021 ± 0.007
14	0.162-0.190	1.015 ± 0.016 ± 0.005
15	0.190-0.227	0.683 ± 0.012 ± 0.005
16	0.227-0.275	0.444 ± 0.008 ± 0.003
17	0.275-0.337	0.282 ± 0.006 ± 0.003
18	0.337-0.418	0.157 ± 0.004 ± 0.002
19	0.418-0.523	0.089 ± 0.003 ± 0.001
bin	range	$(1/\sigma) \times (d\sigma/d\phi^*_\eta)$ ($\times$1000)
20	0.523-0.657	45.296 ± 1.581 ± 0.371
21	0.657-0.827	22.931 ± 1.019 ± 0.113
22	0.827-1.041	10.886 ± 0.636 ± 0.092
23	1.041-1.309	4.909 ± 0.378 ± 0.114
24	1.309-1.640	2.848 ± 0.262 ± 0.073
25	1.640-2.049	1.330 ± 0.161 ± 0.045
26	2.049-2.547	0.921 ± 0.120 ± 0.044
27	2.547-3.151	0.363 ± 0.069 ± 0.019
28	3.151-3.878	0.226 ± 0.051 ± 0.010
29	3.878-4.749	0.214 ± 0.048 ± 0.013

TABLE IV: The corrected $(1/\sigma) \times (d\sigma/d\phi^*_\eta)$ distribution for the dielectron channel and $|y| > 2$.

bin	range	$(1/\sigma) \times (d\sigma/d\phi^*_\eta)$
1	0.000-0.010	15.625 ± 0.361 ± 0.031
2	0.010-0.020	14.288 ± 0.344 ± 0.023
3	0.020-0.030	12.130 ± 0.319 ± 0.030
4	0.030-0.040	9.514 ± 0.281 ± 0.027
5	0.040-0.050	7.572 ± 0.250 ± 0.009
6	0.050-0.060	6.311 ± 0.226 ± 0.016
7	0.060-0.071	5.052 ± 0.202 ± 0.013
8	0.071-0.081	3.991 ± 0.175 ± 0.008
9	0.081-0.093	3.206 ± 0.152 ± 0.008
10	0.093-0.106	2.533 ± 0.126 ± 0.006
11	0.106-0.121	1.796 ± 0.099 ± 0.006
12	0.121-0.139	1.658 ± 0.087 ± 0.006
13	0.139-0.162	1.223 ± 0.067 ± 0.002
14	0.162-0.190	0.767 ± 0.047 ± 0.005
15	0.190-0.227	0.605 ± 0.037 ± 0.003
16	0.227-0.275	0.378 ± 0.025 ± 0.003
17	0.275-0.337	0.195 ± 0.016 ± 0.002
18	0.337-0.418	0.114 ± 0.011 ± 0.001
19	0.418-0.523	0.050 ± 0.006 ± 0.001
bin	range	$(1/\sigma) \times (d\sigma/d\phi^*_\eta)$ (×1000)
20	0.523-0.657	24.457 ± 3.781 ± 0.616
21	0.657-0.827	4.145 ± 1.382 ± 0.122
22	0.827-1.041	2.906 ± 1.099 ± 0.148
23	1.041-1.309	0.503 ± 0.356 ± 0.024
24	1.309-1.640	0.154 ± 0.154 ± 0.014
25	1.640-2.049	0.101 ± 0.101 ± 0.009

TABLE V: The corrected $(1/\sigma) \times (d\sigma/d\phi^*_\eta)$ distribution for the dimuon channel and $|y| < 1$.

bin	range	$(1/\sigma) \times (d\sigma/d\phi^*_\eta)$
1	0.000-0.010	12.992 ± 0.058 ± 0.027
2	0.010-0.020	11.958 ± 0.055 ± 0.022
3	0.020-0.030	10.263 ± 0.051 ± 0.015
4	0.030-0.040	8.620 ± 0.047 ± 0.013
5	0.040-0.050	7.115 ± 0.043 ± 0.010
6	0.050-0.060	5.863 ± 0.039 ± 0.007
7	0.060-0.071	4.868 ± 0.035 ± 0.006
8	0.071-0.081	4.084 ± 0.031 ± 0.006
9	0.081-0.093	3.400 ± 0.027 ± 0.005
10	0.093-0.106	2.831 ± 0.024 ± 0.004
11	0.106-0.121	2.320 ± 0.020 ± 0.003
12	0.121-0.139	1.850 ± 0.016 ± 0.003
13	0.139-0.162	1.439 ± 0.013 ± 0.003
14	0.162-0.190	1.061 ± 0.010 ± 0.002
15	0.190-0.227	0.779 ± 0.007 ± 0.002
16	0.227-0.275	0.526 ± 0.005 ± 0.002
17	0.275-0.337	0.331 ± 0.004 ± 0.001
18	0.337-0.418	0.207 ± 0.003 ± 0.001
19	0.418-0.523	0.117 ± 0.002 ± 0.001
bin	range	$(1/\sigma) \times (d\sigma/d\phi^*_\eta)$ ($\times$1000)
20	0.523-0.657	66.026 ± 1.160 ± 0.479
21	0.657-0.827	34.188 ± 0.753 ± 0.304
22	0.827-1.041	17.056 ± 0.480 ± 0.256
23	1.041-1.309	8.753 ± 0.315 ± 0.254
24	1.309-1.640	4.774 ± 0.214 ± 0.130
25	1.640-2.049	2.489 ± 0.139 ± 0.073
26	2.049-2.547	1.394 ± 0.096 ± 0.044
27	2.547-3.151	0.802 ± 0.066 ± 0.025
28	3.151-3.878	0.536 ± 0.051 ± 0.025
29	3.878-4.749	0.307 ± 0.034 ± 0.012

TABLE VI: The corrected $(1/\sigma) \times (d\sigma/d\phi^*_\eta)$ distribution for the dimuon channel and $1 < |y| < 2$.

bin	range	$(1/\sigma) \times (d\sigma/d\phi^*_\eta)$
1	0.000-0.010	13.404 ± 0.105 ± 0.051
2	0.010-0.020	12.008 ± 0.100 ± 0.026
3	0.020-0.030	10.647 ± 0.094 ± 0.016
4	0.030-0.040	8.755 ± 0.086 ± 0.013
5	0.040-0.050	7.230 ± 0.077 ± 0.016
6	0.050-0.060	5.804 ± 0.069 ± 0.019
7	0.060-0.071	4.972 ± 0.063 ± 0.011
8	0.071-0.081	4.045 ± 0.056 ± 0.008
9	0.081-0.093	3.441 ± 0.050 ± 0.008
10	0.093-0.106	2.820 ± 0.043 ± 0.009
11	0.106-0.121	2.330 ± 0.036 ± 0.006
12	0.121-0.139	1.824 ± 0.029 ± 0.004
13	0.139-0.162	1.414 ± 0.023 ± 0.003
14	0.162-0.190	1.066 ± 0.018 ± 0.002
15	0.190-0.227	0.756 ± 0.013 ± 0.001
16	0.227-0.275	0.514 ± 0.009 ± 0.002
17	0.275-0.337	0.326 ± 0.007 ± 0.002
18	0.337-0.418	0.200 ± 0.005 ± 0.001
19	0.418-0.523	0.107 ± 0.003 ± 0.000
bin	range	$(1/\sigma) \times (d\sigma/d\phi^*_\eta)$ ($\times$1000)
20	0.523-0.657	54.251 ± 1.874 ± 0.638
21	0.657-0.827	25.906 ± 1.162 ± 0.259
22	0.827-1.041	12.306 ± 0.730 ± 0.261
23	1.041-1.309	5.197 ± 0.439 ± 0.174
24	1.309-1.640	2.536 ± 0.279 ± 0.085
25	1.640-2.049	1.263 ± 0.206 ± 0.086
26	2.049-2.547	0.503 ± 0.113 ± 0.038
27	2.547-3.151	0.350 ± 0.104 ± 0.022
28	3.151-3.878	0.209 ± 0.063 ± 0.014
29	3.878-4.749	0.069 ± 0.042 ± 0.012